Magnetic Resonance in Medical Sciences, Vol. 4, No. 3, p. 137–143, 2005

TECHNICAL NOTE

Development of a Compact Mouse MRI Using a Yokeless Permanent Magnet

Tohru SHIRAI[1], Tomoyuki HAISHI[2], Shin UTSUZAWA[1,2], Yoshimasa MATSUDA[1], and Katsumi KOSE[1]*

[1]*Institute of Applied Physics, University of Tsukuba*
1-1-1 Tennodai, Tsukuba, Ibaraki 305-8573, Japan
[2]*MRTechnology Incorporated, Tsukuba, Japan*
(Received July 6, 2005; Accepted September 29, 2005)

A compact mouse MRI has been developed using a 1.0T yokeless permanent magnet and portable MRI console. The entire system was installed in a space measuring 2 m × 1 m. The imaging region was the cylindrical volume (35 mm diameter, 50 mm length) at the center of the magnet and was used for whole-brain or body imaging of mice. Whole-brain imaging took less than 90 min for T_1- and T_2-weighted 3D images with 2-mm slice thickness and 200-μm in-plane resolution. Body imaging took less than 30 min for T_1-weighted spin-echo and FLASH 3D images with 0.5- to 1.0-mm slice thickness and 250- to 300-μm in-plane resolution. In addition to the compactness of the system, the mouse MRI has several advantages over high-field superconducting animal MRI systems in its accessibility to the specimen, similarity to clinical MRI in image contrast, capacity for biological isolation, and maintenance. The results obtained demonstrate the potential of this new system for routine imaging in biomedical laboratories.

Keywords: ***mouse, permanent magnet, compact MRI, Mn-enhanced MRI***

Introduction

The number of MR imaging studies in mice is increasing rapidly, primarily because transgenic mice have become widely available. In most such studies, MR imaging of animals employs a system with a high-field (>4.7T) superconducting magnet, or a 1.5T whole-body clinical MRI is used. However, if a biomedical laboratory wishes to introduce its own system for MR imaging of mice, neither of these systems is suitable because they require a large installation space.

Recently, with progress in design technology for clinical permanent magnets, compact and high-field (~1.0T) permanent magnet circuits have become available for MRI.[1–4] The new magnets have no yokes and comprise permanent magnet material blocks. We report a compact system for MRI of mice that uses a yokeless permanent magnet that can be installed even in small laboratories.[5,6]

*Corresponding author, Phone: +81-29-853-5214, Fax: +81-29-853-5205, E-mail: kose@bk.tsukuba.ac.jp

Materials and Methods

Compact Mouse MRI

Figure 1a is an overview of the compact MRI for mice that was developed in this study. The system consists of a yokeless permanent magnet (NEOMAX Co., Ltd., Osaka, Japan), gradient coil assembly, radiofrequency (RF) probe, and portable MRI console.[7,8] The entire system was installed in a space measuring 2 m × 1 m.

Figure 1b shows the structure of the yokeless permanent magnet. The magnet comprises Fe–Nd–B permanent magnet blocks that form a ''magic sphere''.[1–4] The magnet blocks were assembled to focus the magnetic flux of the magnetic material to the magnet gap. The size and weight of the magnet was reduced drastically by this yokeless magnet design because the iron yokes of conventional (yoked) MRI magnets are substantial. The specifications of the yokeless magnet are: field strength, 1.04T at 25°C; gap, 9 cm; homogeneity, 10 ppm over 30 mm dsv; magnet size, 57.4 cm (W) × 52 cm (H) × 48 cm (D); and weight, ~980 kg. Because the magnet has a 9-cm high, 24-cm wide, and 48-cm deep air gap, access to the sample is very easy.

a

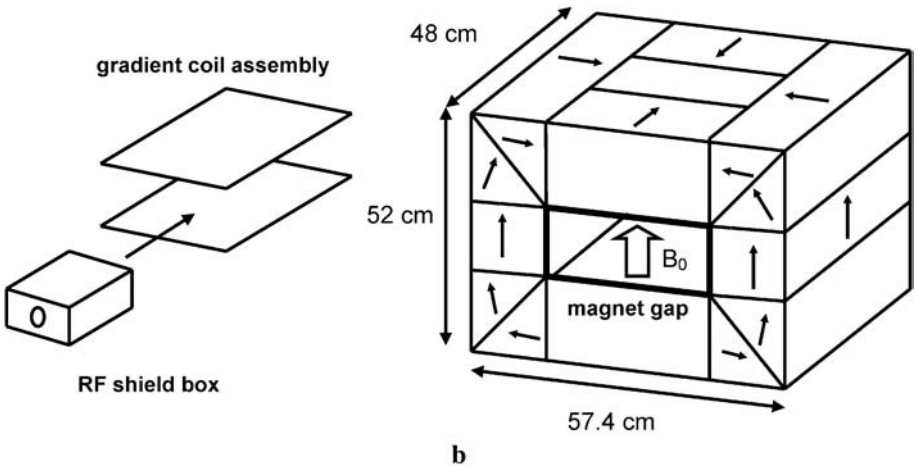

b

Fig. 1.
a: Overview of the compact mouse MRI. On the left is the permanent magnet covered with slabs of polystyrene foam to avoid temperature drift; on the right is the portable MRI console.
b: Schematic drawings of the RF shield box, gradient coil assembly, and yokeless permanent magnet circuit. The RF shield box and gradient coil assembly were fixed in the square gap of the magnet. Each magnet block is made of Fe–Nd–B permanent magnet material. The arrows show the direction of magnetization of the material.

A home-built planar gradient coil set was fixed on the faces of the pole pieces of the magnet. An RF shield box made of 0.3-mm-thick brass plates was fixed between the gradient coil planes. An 8-turn solenoid coil (32 mm diameter, 50 mm length) was fixed at the center of the RF shield box for brain imaging of mice. Another RF shield box with an RF solenoid coil with a larger bore was used for body imaging of mice and phantoms.

Measurements of Permanent Magnet Performance

To measure the temporal stability and spatial homogeneity of the permanent magnet, 2 experiments were performed. The first involved long-term measurements of the Larmor frequency and temperature of the magnet when the imaging gradients were turned on and off. The second involved imaging water phantoms to measure the size of the available field of view (FOV) for imaging mice. Two water phantoms were prepared for the above experiments as follows. Using 2 tube containers (39-mm outer diameter [OD], 35-mm inner diameter [ID]), acrylic pipes (6.0-mm OD, 4.0-mm ID) were closely packed in one tube with the pipe axes parallel to the tube axis, and in the other tube with the pipe axes perpendicular to the tube axis. The tubes were filled with $CuSO_4$-doped water.

Animals and Anesthesia

Animal studies were performed under the guide-

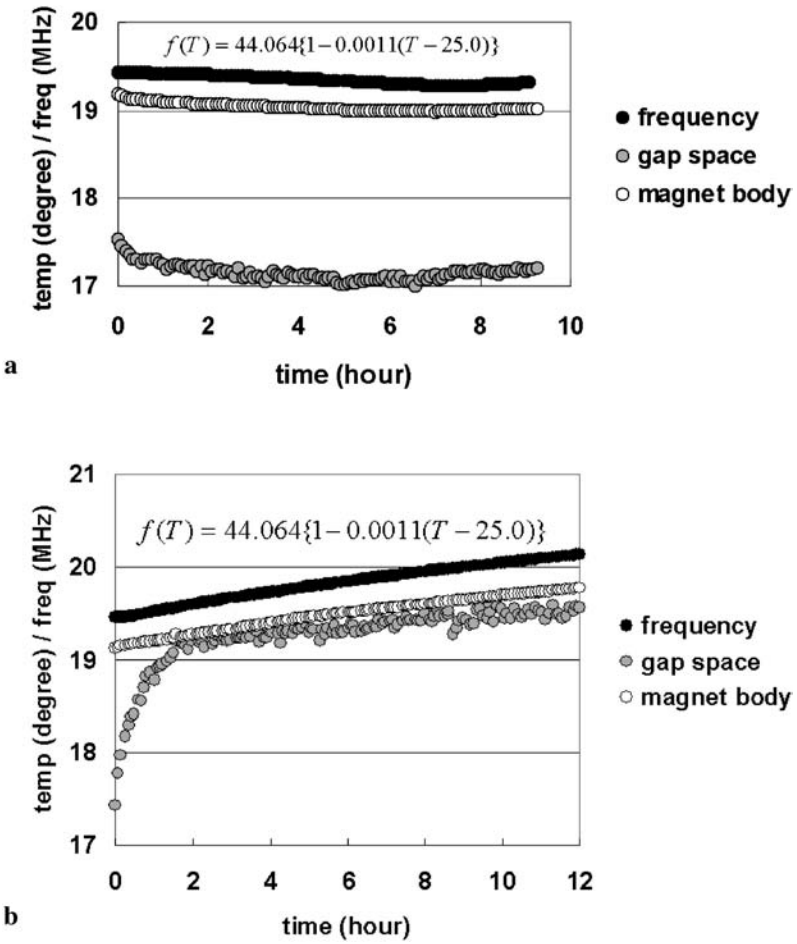

Fig. 2. Larmor frequency and temperature of the permanent magnet measured when a 3D spin-echo imaging sequence was applied. The temperature was measured at 2 locations, on the side of the magnet and at the magnet gap space.
a: Magnetic field gradients were turned off.
b: Magnetic field gradients were turned on.

line of the University of Tsukuba. Male ICR mice (8 to 13 weeks old) were used for MRI studies. One mouse received 0.6 mL of an equal-volume mixture of 0.8% $MnCl_2$ solution and 1.9% glucose solution via subcutaneous injection.[9]

Mice were anesthetized with isoflurane (3 ~ 5%) in air. To maintain anesthesia, the volume of isoflurane relative to the air was reduced to 0.5 ~ 1.5%. After anesthesia, the mice were placed in a custom-designed mouse holder to fit inside the RF coil. Mice were imaged using 3D spin-echo or 3D FLASH sequences with an internal nuclear magnetic resonance (NMR) lock technique described previously.[8] All the mice recovered after imaging experiments of a few hours.

Results

Measurements of Permanent Magnet Performance

Figure 2 shows the Larmor frequency and temperature of the magnet measured for about half a day when a 3D spin-echo imaging sequence (repetition time [TR] = 100 ms, echo time [TE] = 12 ms) was applied. The temperature was measured at 2 locations, on the side of the magnet using Pt resistance thermosensors and at the magnet gap space using a thermocouple. Figure 2a shows the dataset when the field gradients were off, and Fig. 2b shows the dataset when the gradients were on.

The Larmor frequency $f(T)$ MHz was plotted as a temperature (T°C) by assuming the following relation: $f(T) = 44.064\{1 - 0.0011(T - 25.0)\}$. This equation is based on Larmor frequency of 44.064 MHz at 25.0°C and the assumption that the

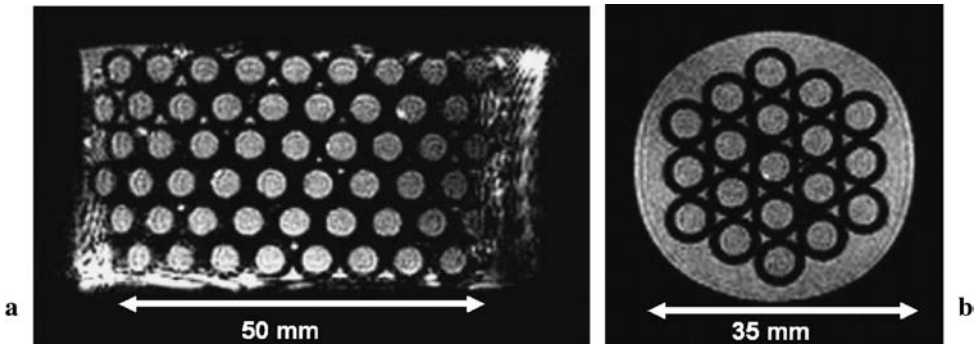

Fig. 3. 2D images of water phantoms selected from 3D-image datasets. Inner diameter of the tube phantom was 35 mm. Outer and inner diameters of the acrylic pipes were 6 mm and 4 mm, respectively.
a: Image in the xy plane.
b: Image in the xz plane.

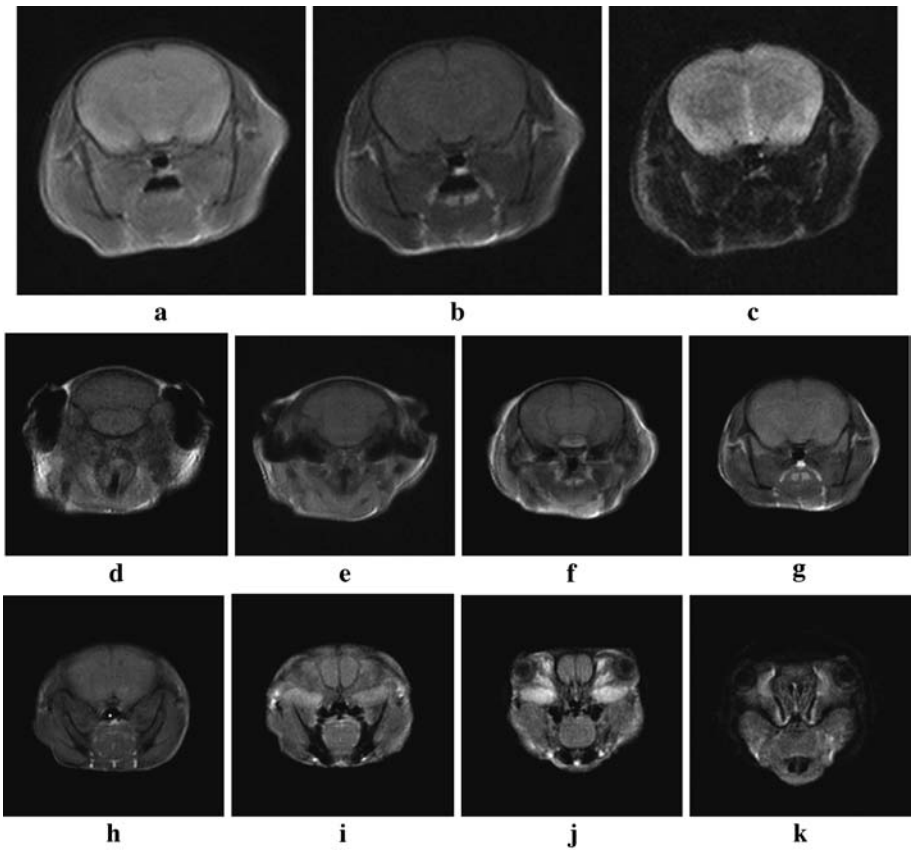

Fig. 4. Spin-echo images of a mouse brain acquired with 3D spin-echo sequences. Field of vision (FOV) 25.6 mm × 25.6 mm × 32 mm; image matrix 128 × 128 × 16; voxel size 200 μm × 200 μm × 2 mm; and NEX = 1.
a: Proton-density-weighted image. Repetition time (TR) = 2000 ms; echo time (TE) = 15 ms; imaging time = 70 min.
b: T_1-weighted image. TR = 500 ms; TE = 15 ms; imaging time = 17 min.
c: T_2-weighted image. TR = 2000 ms; TE = 80 ms; imaging time = 70 min.
d–**k**: Contiguous slices acquired with the same T_1-weighted 3D spin-echo sequence (TR = 500 ms; TE = 15 ms; imaging time = 17 min) as in **b**.

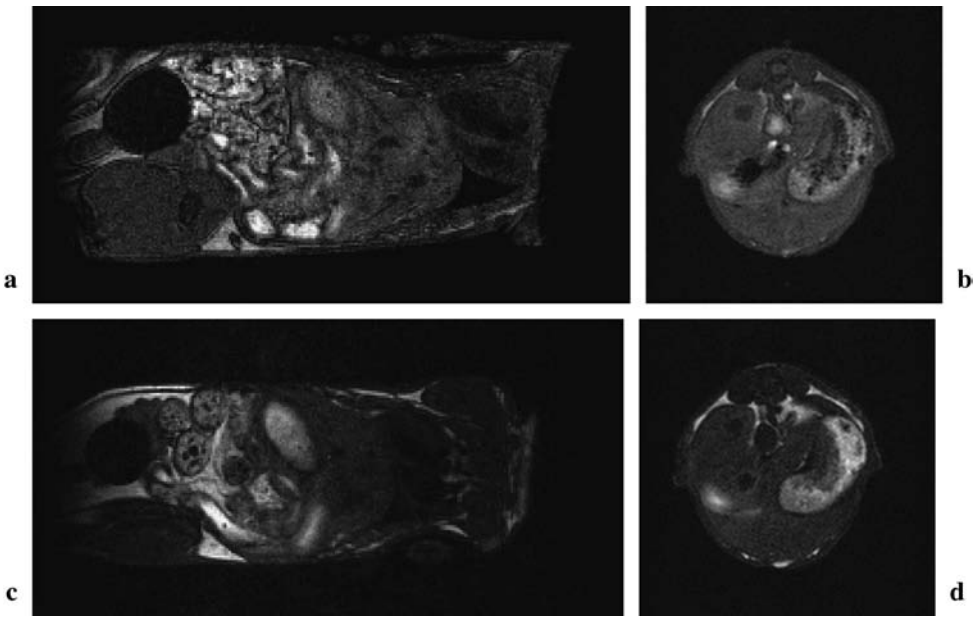

Fig. 5. 2D images selected from 3D-image datasets of a mouse body.
a: Coronal FLASH image. Repetition time (TR) = 30 ms; echo time (TE) = 5 ms; FA = 50°; field of vision (FOV) 64 mm × 32 mm × 32 mm; image matrix 256 × 128 × 64; voxel size 250 μm × 250 μm × 0.5 mm; NEX = 2; imaging time = 14 min.
b: Axial FLASH image. TR = 30 ms; TE = 5 ms; FA = 60°; FOV 38.4 mm × 38.4 mm × 32 mm; image matrix 128 × 128 × 32; voxel size 300 μm × 300 μm × 1 mm; NEX = 1; imaging time = 3 min.
c: Coronal spin-echo image. TR = 100 ms; TE = 10 ms; FOV 76.8 mm × 38.4 mm × 32 mm; image matrix 256 × 128 × 32; voxel size 300 μm × 300 μm × 1 mm; NEX = 1; imaging time = 7 min.
d: Axial spin-echo image. TR = 100 ms; TE = 15 ms; FOV 38.4 mm × 38.4 mm × 32 mm; image matrix 128 × 128 × 32; voxel size 300 μm × 300 μm × 1 mm; NEX = 1; imaging time = 7 min. **b** and **d** are the same cross section.

temperature coefficient of the magnetic flux density of the permanent magnet is −1100 ppm/deg.[10] Figure 2 clearly shows that the magnetic field gradients considerably affect the magnet temperature and Larmor frequency (magnetic field strength).

Figure 3 shows 2D images of water phantoms selected from 3D-image datasets acquired with 3D spin-echo imaging sequences. Although the homogeneity (10 ppm) of the magnet was guaranteed only in the central 30-mm dsv, these results clearly demonstrate that the cylindrical region (35-mm diameter, 50-mm length) can be used to image mice.

Mouse Imaging

Figure 4 shows 2D images of a mouse brain selected from 3D-image datasets acquired with 3D spin-echo sequences. All images were acquired with the following parameters: FOV, 25.6 mm × 25.6 mm × 32 mm; image matrix, 128 × 128 × 16; voxel size, 200 μm × 200 μm × 2 mm; and number of excitations (NEX) = 1. Figures 4a, b, and c show a proton-density-weighted image, T_1-weighted image, and T_2-weighted image of the same slice. Imaging times for Figs. 4a, b, and c were about 70, 17, and 70 min, respectively. Figures 4d through k show contiguous slices acquired with the same T_1-weighted 3D spin-echo sequence as that of Fig. 4b.

Figure 5 shows 2D images selected from 3D-image datasets of a mouse body acquired without respiratory gating. Figures 5a and b were acquired with 3D FLASH sequences and 5c and d with 3D spin-echo sequences. Imaging times for Figs. 5a, b, c, and d were 14, 3, 7, and 7 min, respectively.

Figure 6 shows cross-sectional images of an $MnCl_2$-treated mouse brain selected from a 3D-image dataset acquired by 3D FLASH sequence (TR = 30 ms, TE = 5 ms, FA = 80°, NEX = 8). The mouse was imaged 8 days after administration of $MnCl_2$. In the coronal plane (Fig. 6a), image intensities at the anterior pituitary and hippocampus are enhanced. In the sagittal plane (Fig. 6b), the olfactory bulb, inferior colliculus, and hippocampus are

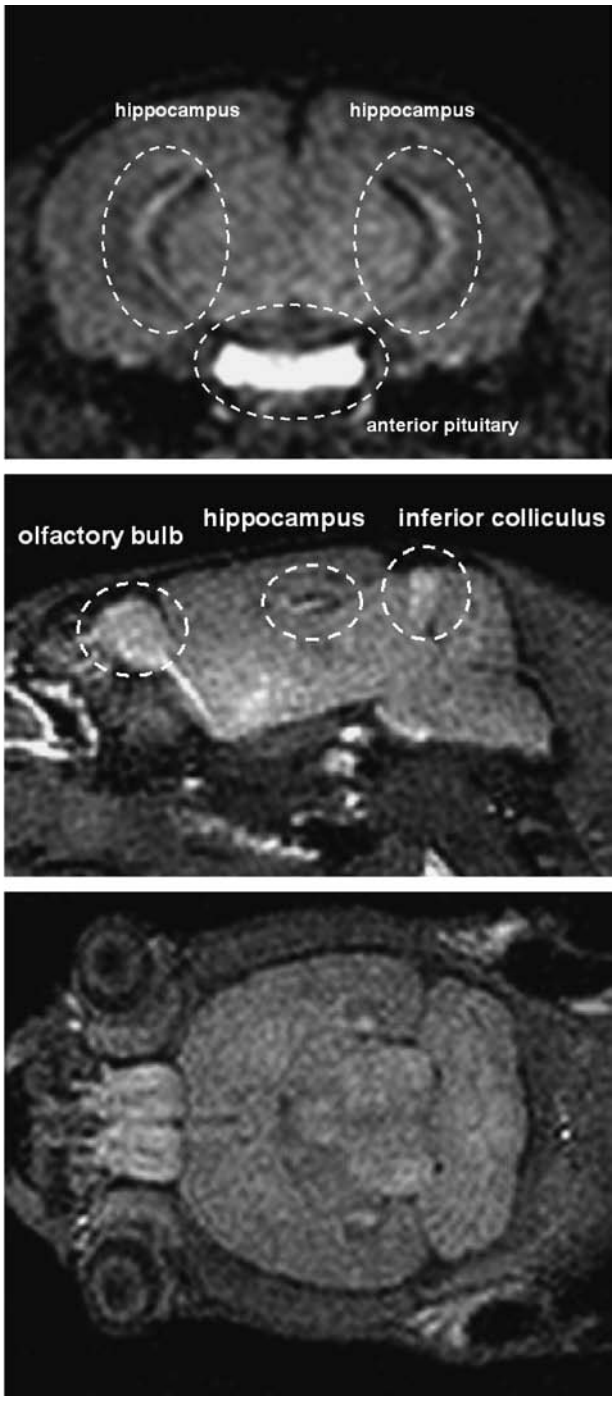

Fig. 6. Cross-sectional images of an $MnCl_2$-treated mouse brain selected from a 3D isotropic image dataset acquired with a 3D FLASH sequence. Repetition time (TR) = 30 ms; echo time (TE) = 5 ms; FA = 80°; NEX = 8; imaging time = 90 min; field of vision (FOV) 51.2 mm × 25.6 mm × 25.6 mm; matrix 256 × 128 × 128; isotropic voxel (200 μm)^3.
a: Coronal plane.
b: Sagittal plane.
c: Axial plane.

clearly visualized.

Discussion

The rate of increase in temperature (~0.07 deg/h) caused by the gradients shown in Fig. 2b can be accounted for quantitatively by the Joule heat of the gradients. The Larmor frequency change of ~3.4 kHz/h, corresponding to ~0.07 deg/h temperature drift, was corrected using a time-sharing internal NMR lock technique described previously.[8] The mouse images presented in Figs. 4 to 6 clearly demonstrate that the NMR lock technique worked quite well in this system.

The results of experiments on phantoms and of mouse coronal body imaging demonstrated that the central cylindrical region (35-mm diameter, 50-mm length) can be used for MR imaging. This region was also used for imaging rat brains,[6] but is not suitable for imaging rat bodies.

In the mouse-imaging experiments, we used 3D imaging instead of multi-slice imaging, which is usually used in clinical MRI. Three-dimensional imaging has several advantages over multi-slice imaging when a number of signal accumulations are inevitable. In our situation, gapless image acquisition was most profitable because slice gap is inevitable in a standard multi-slice imaging procedure. Although the solenoid coil has about a 2- to 3-fold SNR advantage over saddle-shaped or birdcage coils,[11] the 1.0T field strength requires signal accumulations of at least several-fold for mouse imaging, in which high spatial resolution is indispensable.

The imaging time of the T_1-weighted sequence was reasonably short for both brain and body imaging, as shown in the preceding section. The imaging time for the T_2-weighted imaging sequence, however, was not short enough for weak mice. Therefore, the T_2-weighted imaging sequence should be shortened using a 3D fast spin-echo sequence or some other faster sequence.

Although the SNR of the MR images obtained with this system may be lower than that achieved with MRI using high-field superconducting magnets, this system has several advantages over such systems. The first is compactness of the system; the entire system was installed in a space 2 m × 1 m compared to more than about 20 m^2 required for an animal MRI system using a high-field superconducting magnet. The second advantage is accessibility to the mouse. Because the distance between the center and the opening of the magnet is only 24 cm and the size of the gap is 24 cm wide by 9 cm high, access to mice is easier than with high-field

superconducting animal MRI systems, in which the distance between the center and opening of the magnet is usually more than 50 cm. The third advantage is similarity of image contrast to that of clinical MRI systems. As is well known, image contrast in MRI is largely affected by resonance frequency (magnetic field strength) because T_1 and T_2* depend on resonance frequency. So, contrast between MR images acquired with high-field animal MRI systems and with clinical MRI systems, which usually use a 1.5T magnetic field, cannot be compared directly. Our system has a certain advantage on this point because the magnetic field strength is close to that of clinical MRI. The fourth advantage is the capability for biological isolation. Not a few biological laboratories using mice require strict biological isolation from the outside environment, so use of superconducting animal MRI systems is difficult because cryogen refill or refrigerator maintenance may destroy the biological isolation. The fifth advantage is magnet maintenance. Although the permanent magnet needs some electrical power to regulate temperature, no cryogen refill or cold-head replacement of the refrigerator is required.

Conclusion

We have developed a compact mouse MRI using a 1.0T yokeless permanent magnet and portable MRI console, and we have demonstrated its potential by imaging several mice. The system's several unique advantages over existing systems for MR imaging of mice recommend its usefulness as a tool for routine imaging in biomedical laboratories.

Acknowledgments

The authors thank Dr. Masae Yaguchi for her helpful advice on the preparation of mice, Drs. Eiichi Fukushima and Steve Altobelli for live mouse experiments, and Mr. Masaaki Aoki and Mr. Tsuyoshi Tsuzaki for constructing the yokeless permanent magnet.

References

1. Halbach K. Design of permanent multipole magnets with oriented rare earth cobalt material. Nucl Instr Meth 1980; 169:1–10.
2. Zijlstra H. Permanent magnet for NMR tomography. Philips J Res 1985; 40:259–288.
3. Leupold HA, Potenziani II E, Abele MG. Applications of yokeless flux confinement. J Appl Phys 1988; 64:5994–5996.
4. Nakanishi A. Development of a very compact high performance magnetic circuit. Transactions of the Institute of Electrical Engineers of Japan 2001; 121-D:715 (in Japanese).
5. Haishi T, Utsuzawa S, Shirai T, et al. Mouse MRI systems using dipole ring permanent magnets, In: Proceedings of the 11th Annual Meeting of ISMRM. Toronto, 2003; 751.
6. Shirai T. Development of a compact MRI for mouse and rat. Master's thesis, 2004, University of Tsukuba.
7. Kose K, Haishi T, Adachi N, Uematsu T, Yoshioka H, Anno I. Development of an MR microscope using a portable MRI unit and a clinical whole body magnet, In: Proceedings of the 7th Annual Meeting of the ISMRM. Philadelphia, 1999; 2036.
8. Haishi K, Uematsu T, Matsuda Y, Kose K. Development of a 1.0T MR microscope using a Nd–Fe–B permanent magnet. Magn Reson Imag 2001; 19:875–880.
9. Watanabe T, Natt O, Boretius S, Frahm J, Michaelis T. *In vivo* 3D MRI staining of mouse brain after subcutaneous application of $MnCl_2$. Magn Reson Med 2002; 48:852–859.
10. Data sheet of permanent magnet materials. Sumitomo Special Metals Company (NEOMAX Co., Ltd.).
11. Houllt DI, Richards RE. The signal-to-noise ratio of the nuclear magnetic resonance. J Magn Reson 1976; 24:71–85.